Dynamical transition on the periodic Lorentz gas: Stochastic and deterministic approaches

Rafael Mateus Feliczaki,[*] Eduardo Vicentini,[†] and Pedro Pablo González-Borrero[‡]

Departamento de Física, Universidade Estadual do Centro-Oeste, Simeão Camargo Varela de Sá 3, 85040-080 Guarapuava PR, Brazil

The effect of dynamical properties of the periodic Lorentz gas on the autocorrelation function and diffusion coefficient are investigated in various geometric transitions between billiards without horizon and infinite horizon. Numerical simulations are performed using a double square lattice which permits us to isolate different types of corridors and to describe the individual effects of each corridor. The results are compared with a stochastic model based on a escape-rate formalism which reveals the sensibility of the diffusion coefficient and clarifies the role of the open corridors mechanism on the dynamical transitions

I. INTRODUCTION

One of the major goals in the study of dynamical systems is to understand how macroscopic physical quantities are affected by the dynamical properties given by the microscopic motion of the particles that compose this system. By dynamical properties we refer to those quantities defined by the behavior of deterministic trajectories on the phase space of the particles, such as ergodicity, mixing, chaos and, mainly, by parameters as the Lyapunov exponent and the Kolmogorov entropy. The physical quantities of interest are usually the transport coefficients, which are macroscopic quantities that characterize a system or process. They can be defined by stochastic models, where they are related to microscopic dynamical quantities treated as random variables. Regarding this, we highlight the paper of Gaspard and Nicolis who present the relationship of diffusion coefficient with Lyapounov exponent and Kolmogorov entropy in a Lorentz gas [1].

The periodic Lorentz gas has been consistently used to understand this connection. As a physical model, it is used to study diffusion in a lattice of scatterers [2], whose core dynamics is simple but displays a number of interesting properties, such as chaos and hyperbolicity [3–8]. This system is defined by noninteracting point masses that move freely inside a periodical arrangement of scatterer disks, often modeled by Sinai billiards [9]. One of the key aspects of the periodic Lorentz gas is that its statistical and dynamical properties are connected to its geometry [4–6], especially the horizon, which defines whether an infinite trajectory (along corridors) with no collisions is possible (called infinite horizon or ∞H) or not (without horizon or 0H). Its dynamics is known to be hyperbolic in 0H and nonhyperbolic in ∞H, where the diffusion coefficient is normal in the former and anomalous in the latter [10,11].

Diffusion in the periodic Lorentz gas is usually defined by the deterministic trajectories using the Einstein-Green-Kubo formula, which defines the diffusion coefficient by an integration of the velocity autocorrelation function $C(t) = \langle \mathbf{v}(0) \cdot \mathbf{v}(t) \rangle$ [where $\mathbf{v}(t)$ is the velocity of the particle at time t] [6]. The interest in this function is how it decays depending on the geometric regime. Exponential decay as an upper bound for $C(t)$ is observed in 0H billiards both analytically and numerically [3,5,10,12]. The integration of $C(t)$ leads to a finite value of the diffusion coefficient when $t \to \infty$ (normal diffusion). Friedman and Martin studied $C(t)$ numerically on a triangular lattice billiards and observed exponential decay for 0H and proposed $1/t$ decay for ∞H billiards at long time [5]. They later conjectured that the origin of the $1/t$ decay was a consequence of a geometric property related to the open corridors of ∞H billiards [13]. This case was consistent with an analytical study carried out by Bleher [6]. By integrating $C(t)$, the diffusion coefficient was numerically observed to be anomalous superdiffusive in the ∞H case [12].

It is not clear, however, how some quantities behave in the transition between 0H and ∞H regimes. In the triangular lattice billiards, Matsuoka and Martin found that $C(t)$ and the diffusion coefficient change smoothly from one geometric regime to the other [12]. On the other hand, Gaspard and Baras described it as a thermodynamic phase transition due to a discontinuity in the Ruelle pressure function [14]. Also, in the scope of stochastic models of billiards, some theoretical and numerical studies show that the survival or decay probabilities in closed billiards with a small hole are also sensitive to internal dynamics, where the presence of an algebraic tail after an exponential decay separates nonhyperbolic from hyperbolic systems [11,15–20].

In the periodic Lorentz gas, the stochastic models are mostly focused on the 0H regime, defining the diffusion based on the random walk of the particle between traps formed by a group of adjacent scatterers [4,21–23]. Recently, Cristadoro *et al.* studied the anomalous diffusion, analyzed the moments of the displacement vector, and proposed a correction to its known logarithmic growth based on a time scale of coexistence of normal and anomalous diffusions [24]. The same authors later developed a stochastic model of Lévy walk for both normal and anomalous diffusion regimes and obtained good agreements with simulation data [25].

In our study, we are interested in investigating the dynamical transition between nonhyperbolic and hyperbolic billiards and its influence in the diffusion coefficient as a relevant physical quantity. When the geometry changes from 0H to ∞H, we look at the algebraic tail of the velocity autocorrelation function considering each type of open corridor allowed by our model, with the assistance of a predicted curve based on the volume of the phase space of the open corridors, as well

---
[*]feliczaki.r.m@gmail.com
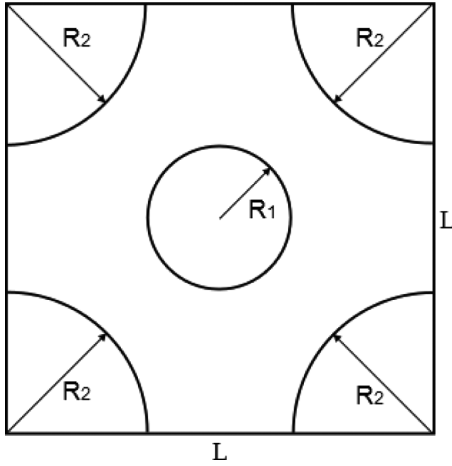[†]evicentini@unicentro.br
[‡]gonzalez@unicentro.br

FIG. 1. Sinai billiard table with length L and two sublattices with radii R_1 and R_2.

FIG. 2. Representation of isolated open corridors in ∞H billiards: (a) bouncing balls; (b) diagonal. In the example (a), the main diagonal corridor (segmented line) is closed by $R_2 > L\sqrt{2}/4$. In (b), the bouncing balls corridors are closed by $R_1 + R_2 > L/2$. In this case, the central disk would touch the corridor if $R_1 = R_2$.

as the behavior of the time-dependent diffusion coefficient. Furthermore, we propose an escape-rate model based on traps formed by adjacent scatterers. It results in an expression for the diffusion coefficient as a function of the survival probability inside the traps and suggests some similarities between the survival probability and the velocity autocorrelation function. We compute all these quantities numerically using a simulator of trajectories in the billiards. Considering the reliability of our mathematical and numerical tools, we extend our investigation from the transition hyperbolic to nonhyperbolic, observing the region where two types of corridors are open, looking for other relevant transitions.

Most of the past studies [1,4–6,9,12–14,21–23] were conducted on a triangular lattice Lorentz gas instead of a square lattice, because in the former it is possible to close all corridors without overlapping the scatterers. One interesting variant of these systems is the double square lattice Lorentz gas with a different radius for each sublattice [10]. Figure 1 represents the unit cell of this lattice characterized by a square box of length L, a central scatterer of radius R_1, and four peripheral scatterers of radius R_2. The major advantage of this lattice is the large geometric variety given by the individual adjustment of the radius of each sublattice, which permits wide control over the open corridors in ∞H billiards. The two types of open corridors that can be isolated in this system are the vertical-horizontal and the main diagonal. Thus, it is possible to analyze how each type of corridors influences the billiard dynamics when the transitions are made from 0H to ∞H billiards by opening one or another corridor.

The paper is organized as follows. In Sec. II, we describe the geometric properties of the billiards, detailing the horizon property and how it relates to the billiard dynamics. The theoretical model is developed in Sec. III, which presents the time-dependent diffusion coefficient formulas in terms of velocity autocorrelation function and survival probability, where the latter is achieved by a escape-rate model. Section IV describes the details of the simulations and the numerical experiments. The results are shown and discussed in Sec. V, describing the unique geometric transitions enabled by the double square lattice. Concluding remarks are made in Sec. VI.
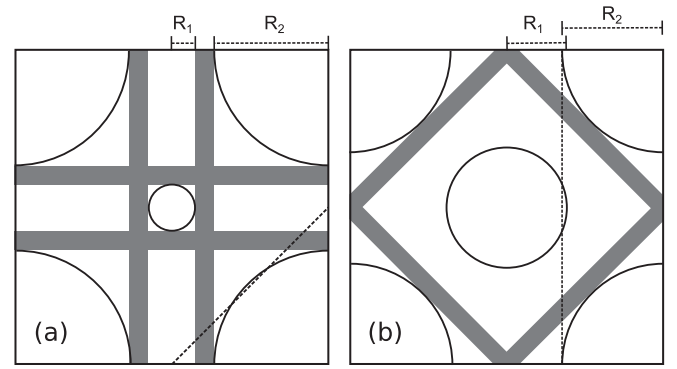
II. GEOMETRIC AND DYNAMICAL PROPERTIES OF BILLIARDS

The horizon is a geometric property defined by the size of the scatterer disks and characterizes the longest straight path that a particle can travel without collisions. In billiards with infinite horizon (∞H), there are open corridors where a trajectory without collisions is possible, such as in Fig. 2. In billiards without horizon (0H), such corridors are closed and a trajectory without collisions is not possible. As a special case of 0H billiards, there is a group of enclosed ones where the boundaries of the scatterer disks touch or overlap each other, what traps the trajectories to a confined space. We consider only the 0H cases where no trajectory is trapped even though all corridors are closed.

In the ∞H case for the double lattice Sinai billiards, there is a possibility of isolating two different types of open corridors. We denominate billiards with only vertical and horizontal corridors as bouncing balls (denoted BB), shown in Fig. 2(a). They occur when either R_1 or $R_2 \geqslant L\sqrt{2}/4$, while $R_1 + R_2 < L/2$. On the other hand, the main diagonal corridor (denoted D) is isolated when both R_1 and $R_2 < L\sqrt{2}/4$, while $R_1 + R_2 \geqslant L/2$ [shown in Fig. 2(b)].

All the possible geometric configurations of the Sinai billiards with two sublattices are shown in Fig. 3 in terms of disk radii relative to the box size. In the lower left region, where both radii are small, are the ∞H billiards with at least two main open corridors (BB and D). For large radii some corridors may close, such as in the striped areas where only the BB corridors are open, and in the checkerboard area where only the D corridors are open. They are bounded by the relations shown in the previous paragraph. In the 0H areas, all corridors are closed but the disks do not touch each other. The regions with diamondlike shapes are the billiards where the disks touch or overlap, and the shapes represent the remaining billiard table where the particles can move. In the top right region, no billiards are possible, since the disks are big enough to occupy the whole box area, leaving no space for the particles.

To achieve our goal of investigating the sensibility of the diffusion coefficient and correlated quantities, we focus our interest in the regions of Fig. 3 where geometric transitions
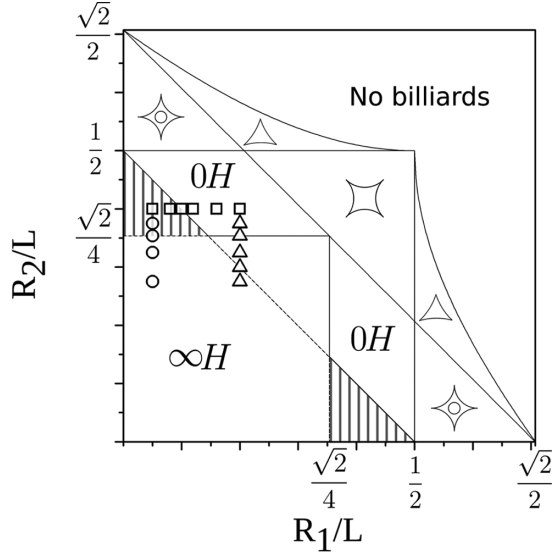
FIG. 3. Classification of the Sinai billiards with two sublattices relative to the radii R_1 and R_2 of the disks. The regions are described in Sec. II. Isolated corridors are located in highlighted areas: stripes for bouncing balls (BB) and checkerboard for diagonal (D). The sequence of small squares, triangles, and circles are the selected configurations for the simulations.
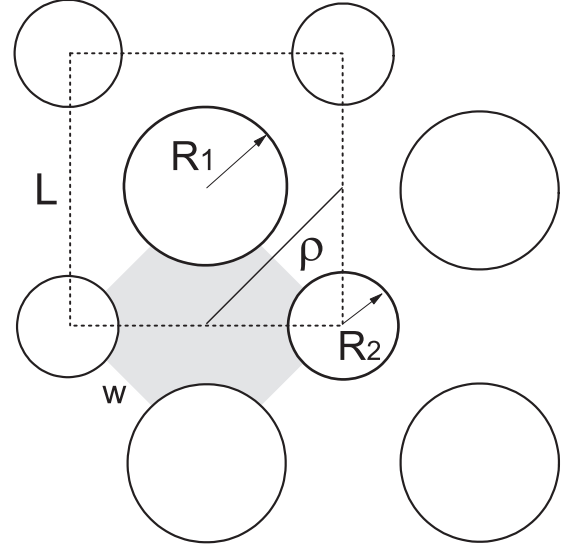

FIG. 4. The dark region delimits the site on the periodic Lorentz gas where the particles spend some time before jumping across the lattice. The segmented square indicates the Sinai billiards, as presented in Fig. 1. w is the distance between two adjacent scatterers and ρ is the distance between two neighboring sites.

between the 0H and the ∞H regimes are found. They can occur either by closing the BB corridors, as shown by the sequence of small squares or by closing the D corridors indicated by the sequence of small triangles. The sequence of small circles passes over a region with a transition from two kinds of open corridors (D and BB) to one kind of open corridor (BB).

The geometric properties are related to the billiard dynamics. All Sinai billiards with any $R > 0$ are fully chaotic, but they are considered fully or strongly hyperbolic only in 0H case [11,16] because all periodic trajectories are isolated with a hyperbolic separation from neighboring trajectories [26]. In the ∞H case, the corridors define a set of nonisolated and nonhyperbolic periodic trajectories, which provide the system with a different long-time behavior for autocorrelation functions and other quantities presented in the Introduction of this paper. Due to the similar behavior to other nonhyperbolic systems, such as nonchaotic billiards (integrable billiards [15,19] and pseudointegrable polygonal billiards [20]), and nonfully chaotic systems [27,28], we adopt the term nonhyperbolic for ∞H billiards and hyperbolic for 0H billiards [16].

III. DETERMINISTIC AND STOCHASTIC APPROACHES TO DIFFUSION

The deterministic approach to diffusion is usually made by applying the Einstein-Green-Kubo formula following the trajectories of the particles in the periodic Lorentz gas. This approach associates the time-dependent diffusion coefficient $D(t)$ with the autocorrelation function $C(t)$ [6]:

$$D(t) = \frac{\langle |\mathbf{r}(t) - \mathbf{r}(0)|^2 \rangle}{4t}$$
$$= \frac{1}{2} \int_0^t C(\xi) d\xi - \frac{1}{2t} \int_0^t \xi C(\xi) d\xi. \quad (1)$$

When the system shows normal diffusion, the diffusion coefficient D is obtained by $D = \lim_{t \to \infty} D(t)$.

The stochastic approach to the Lorentz gas has been made by considering that a particle spends some time trapped in a site between a group of neighboring scatterers and jumps to other sites in a random walk manner. For a two-dimensional system, the diffusion coefficient is known [29] as

$$D = \frac{\ell^2}{4\tau}, \quad (2)$$

where ℓ is the mean length of jumps between sites and τ is the mean time spent between jumps. For the 0H periodic Lorentz gas, Machta and Zwanzig [4] used $\ell = \rho$, the distance between the centers of two neighboring sites and the mean time

$$\tau = \frac{\pi A}{P}, \quad (3)$$

where A is the area of the site and P is the perimeter where the particles cross or collide [8]. Using the same proposal for our arrangement of scatterers, $\ell = L/\sqrt{2}$ and

$$\tau = \tau_e = \frac{\pi \left[L^2 - \pi \left(R_1^2 + R_2^2 \right) \right]}{8 [L/\sqrt{2} - (R_1 + R_2)]}. \quad (4)$$

In the latter, τ_e is taken as a mean escape time, which is described below.

In Fig. 4, the dark region represents one site where the particles spend a specific amount of time colliding with neighboring scatterers before jumping to another site. For (4), the area A of the dark region is a half of the Sinai billiards (Fig. 1) and the perimeter is $P = 4w = 4[L/\sqrt{2} - (R_1 + R_2)]$. Numerical simulations for D show that the result in (2) is better for small values of w [4]. Recent papers [23,24] introduce improvements to obtain ℓ and τ in (2), obtaining suitable fits for numerical results.

Our approach uses the continuous time random walk method [30] to introduce the probability density functions: $\phi(t)$ of surviving in the site until time t, $\psi(\mathbf{r},t)$ of jumping with length and direction given by $\mathbf{r}$ after waiting a time t, and $\lambda(\mathbf{r},t)$ of finding the particle at position $\mathbf{r}$ at time t. These probabilities are related by [30,31]:

$$\lambda(\mathbf{r},t) = \int_0^t \eta(\mathbf{r},t')\phi(t - t')dt', \qquad (5)$$

where

$$\eta(\mathbf{r},t) = \int d\mathbf{r}' \int_0^\infty dt' \, \eta(\mathbf{r}',t')\psi(\mathbf{r} - \mathbf{r}',t - t') + \delta(\mathbf{r})\delta(t) \qquad (6)$$

is the probability density function of just having arrived at position $\mathbf{r}$ at time t, after coming from $\mathbf{r}'$ and t'. The delta functions in (6) express the initial conditions. Thereby, (5) is the probability density function of remaining in position $\mathbf{r}$ until time t after arriving at time t'. The Fourier and Laplace transforms of (5) and (6) result in

$$\Lambda(\mathbf{k},u) = \frac{\Phi(u)}{1 - \Psi(\mathbf{k},u)}, \qquad (7)$$

where the uppercase letters stand for the Fourier and Laplace transforms of equivalent probability density funtions, which were presented in lowercase letters [32]. The time-dependent diffusion coefficient is given by [30,31]

$$\begin{aligned} D(t) &= \frac{1}{4t} \int d\mathbf{r} \, r^2 \lambda(\mathbf{r},t) = \frac{1}{4t}\mathcal{L}^{-1}\left\{ \int d\mathbf{r} \, r^2 \Lambda(\mathbf{r},u) \right\} \\ &= \frac{1}{4t}\mathcal{L}^{-1}\left\{ \lim_{k\to 0} \int d\mathbf{r} \, r^2 e^{i\mathbf{k}\cdot\mathbf{r}} \Lambda(\mathbf{r},u) \right\} \\ &= \frac{1}{4t}\mathcal{L}^{-1}\left\{ -\lim_{k\to 0} \frac{\partial^2}{\partial k^2} \Lambda(\mathbf{k},u) \right\}, \end{aligned} \qquad (8)$$

where $\mathcal{L}^{-1}$ stands for inverse Laplace transform. In this approach, the mean quantities ℓ and τ are obtained by

$$\ell^2 = \int_0^\infty 2\pi r dr \, r^2 \int_0^\infty dt \, \psi(r,t) \qquad (9)$$

and

$$\tau = \int_0^\infty dt \, t \int_0^\infty 2\pi r dr \, \psi(r,t). \qquad (10)$$

Using the results shown in Appendix A, (8) reduces to

$$D(t) = \frac{1}{4t}\frac{\ell^2}{\tau^2}\mathcal{L}^{-1}\left\{ \frac{\Phi(u)}{u^2} \right\} \qquad (11)$$

and the inverse Laplace transform is the convolution [32]

$$\mathcal{L}^{-1}\left\{ \frac{\Phi(u)}{u^2} \right\} = \int_0^t (t - s)\phi(s) \, ds. \qquad (12)$$

The final expression for $D(t)$ is

$$D(t) = \frac{\ell^2}{2\tau^2}\left[\frac{1}{2}\int_0^t \phi(\xi) \, d\xi - \frac{1}{2t}\int_0^t \xi\phi(\xi) \, d\xi \right], \qquad (13)$$

which is similar to (1).

In (13), $\phi(t)$ assumes the main role in the determination of $D(t)$. The exponential decay of survival probability $\phi(t) =$

$e^{-t/\tau}$ leads to the diffusion coefficient $D = \lim_{t\to\infty} D(t) = \ell^2/4\tau$ [Eq. (2)], and a possible algebraic decay $\phi(t) \sim \tau/t$, for $t \gg \tau$, leads to logarithmic time-dependent diffusion coefficient $D(t) \sim (\ell^2/4\tau)\ln t/\tau$. However, we can propose the following shape of survival probability:

$$\phi(t) = (1 - B)e^{-t/\tau} + \frac{B}{1 + t/\tau}, \qquad (14)$$

where B is the statistical weight of the algebraic tail. The survival probability with an exponential to algebraic transition was observed by Fendrik and coauthors in Sinai well billiards [11,16], with open corridors, and they associated the trajectories that remain for a long time in corridors with the algebraic tail. Following the suggestions in Refs. [12,13] for autocorrelation functions, we propose the value of B as the relative volume of the open corridors in the phase space in relation to the whole billiard phase space, demonstrated in Appendix B,

$$B = \frac{4c^2}{\pi\left[L^2 - \pi\left(R_1^2 + R_2^2\right)\right]}, \qquad (15)$$

where c is the width of an open corridor.

Using (14) in (13), we obtain

$$\begin{aligned} D(t) = \frac{\ell^2}{4\tau}\bigg\{ &(1 - e^{-t/\tau})(1 - B) + B\left[\ln\left(1 + \frac{t}{\tau}\right) - 1 \right] \\ &+ \frac{\tau}{t}\left[1 - \left(1 + \frac{t}{\tau}\right)e^{-t/\tau} \right](1 + B) \\ &+ \frac{B\tau}{t}\ln\left(1 + \frac{t}{\tau}\right) \bigg\}, \end{aligned} \qquad (16)$$

which has the limit for $t \gg \tau$

$$D(t) = \frac{\ell^2}{4\tau}\left\{ 1 + B\left[\ln\left(\frac{t}{\tau}\right) - 2 \right] \right\}. \qquad (17)$$

In (17), the first constant term is equal to the normal diffusion coefficient [Eq. (2)] and the second term, with the logarithmic function, is proportional to B. We highlight that B coefficient controls the sensibility of $D(t)$ towards the changes in the dynamics of the billiards, since $B = 0$ indicates hyperbolic billiards and $B > 0$ nonhyperbolic billiards.

The results in (17) and (15) are very similar to those obtained by Cristadoro *et al.* [24,25]. In Ref. [24], based on previous results (Ref. [33]), the authors use $D(t) \sim 2\xi_{\text{flow}} \log t$, where the variance ξ_{flow} [34], except for some differences in geometry, corresponds to our $B/4$. However, the ξ_{flow} proposed in Ref. [24] accumulates the contribution of all open corridors whereas we consider separately the contribution of each corridor. Regarding Ref. [25], the authors deduce the diffusion coefficient as $D(t) = (\ell^2/4\tau_R)\{1 + (\delta/\ell)[\ln t + O(1)]\}$ with a constant and a logarithmic part similar to (17), where τ_R was defined as the residence time, equal to our τ_e in (4). Their weight for the logarithmic part is δ/ℓ, where δ is the corridor width which, in their choice of geometry (square lattice), coincides with our c. ℓ is the length of their billiards but also the mean length of jumps and coincides with τ_F, defined by them as the mean time "of propagation across a cell." In order

to compare, we can rewrite (15) as $B = c/\tau_t$, with

$$\tau_t = \frac{\pi\left[L^2 - \pi\left(R_1^2 + R_2^2\right)\right]}{4c}. \tag{18}$$

Herein we call τ_t as the mean time to cross a section of width $4c$, which could be understood as the transition time when moving into corridors. Thus, our B carries a characteristic time, as Ref. [25], but with a different interpretation. Further discussions are presented in Sec. V D together with our results.

IV. NUMERICAL METHODS

The billiard table was defined as a square box of side $L = 1$, with one scatterer disk of radius R_1 in the center of the box, and four disks of radius R_2 centered in each corner of the box, as shown in Fig. 1. Periodical boundary conditions were applied on the sides of the box. The initial conditions of the particles are uniformly random and given by x, y and θ, being (x,y) in the space between the scatterers, and $\theta \in [0,2\pi[$ the angle between the velocity and the horizontal axis x and taking the origin of the coordinate system in the center of the box. We consider particles with unit mass and unit velocity. The collisions are detected by the intersection of the trajectory line with the circle boundary (in collisions with the scatterers) or with the side of the box.

The velocity autocorrelation function is evaluated at each time step by the equation

$$C(t) = \langle\mathbf{v}(0) \cdot \mathbf{v}(t)\rangle = 2\langle v_x(0) \cdot v_x(t)\rangle, \tag{19}$$

being $v_x = \cos(\theta)$ the x component of velocity. Since the billiards show symmetry between x and y coordinates, we assume that the y contribution to the velocity autocorrelation function is equal to the x contribution, thus the right-hand side of Eq. (19) is multiplied by 2. By making $\langle\cdot\rangle$ an average of trajectories of N particles, the Eq. (19) is

$$C(t) = 2\frac{1}{N}\sum_{n=1}^{N}\cos(\theta_{n0})\cos(\theta_{nt}), \tag{20}$$

where the coordinates θ_{n0} and θ_{nt} refer to nth particle at initial and t time, respectively. The number of particles on each simulation for the velocity autocorrelation function was 2×10^7.

The time-dependent diffusion coefficient curve is obtained by numerical integration of the velocity autocorrelation function data following (1) rather than (13), because the former does not use ℓ^2 and τ.

The survival probability $\phi(t)$ was obtained counting the number of particles inside or linked to the original site, as shown in Fig. 4, at each time step. Each particle was followed until it hit a scatterer of another site. In this way, if a particle crosses the lattice using an open corridor, then the computer program considers this particle to be linked with the original site. In order to compare with the autocorrelation function, the simulations for $\phi(t)$ used 10^6 particles (Figs. 5, 6, 8, 9, 11, and 12). To evaluate the behavior of the B parameter in (14) and (17), we used 10^7 particles, whose results are shown in Figs. 14, 15, and 16. In both sets, the measures are averages of 10 simulations for each configuration, with error given by the standard deviation.

V. RESULTS AND DISCUSSION

In the sequence, we show our results on three sets of configurations, represented by each symbol in Fig. 3. Each set keeps the radius of one disk constant while changing the other in order to investigate a particular geometric transition. Hence we show our results in terms of critical radius R_c for geometric transition.

Although the plots for the velocity autocorrelation function and survival probability are shown in reduced units by the mean escape time τ_e [Eq. (4)], we also use the mean collision time τ_c [8],

$$\tau_c = \frac{L^2 - \pi\left(R_1^2 + R_2^2\right)}{2(R_1 + R_2)}, \tag{21}$$

as a reference to the velocity autocorrelation function decay and the diffusion coefficient. We use $P = 2\pi(R_1 + R_2)$, the perimeter of the scatterers inside Sinai billiards, according to (3).

A. 0H to BB

In the first set, the transition from 0H to ∞H is investigated with the bouncing balls corridor being the first to be opened. We fix $R_2 = 0.40L$ and begin with $R_1 = 2.00R_c$ followed by $1.60R_c$, $1.20R_c$, $1.00R_c$, $0.80R_c$, and $0.50R_c$ (represented by squares in Fig. 3), where $R_c = 0.10L$. The BB and 0H billiards are below and above the transition, respectively.

Figure 5 shows the di-log plot of the absolute value of the velocity autocorrelation function $C(t)$ (dots) and the survival probability $\phi(t)$ (squares) of a representative case for 0H billiards, with $1.20R_c$. Since there are no open corridors, the decay of both curves is expected to be purely exponential, as indicated by the dashed curves. The decay rate for the velocity autocorrelation function was fitted to $a = 2.33 \pm 0.01$, using the best fit for the selected points, on the peak of each oscillation (triangles) [35]. The sign changes produce the oscillatory behavior of $C(t)$, which has been explained by the sequence of disk collisions of trajectories [12,13]. Around $10\tau_e$, the exponential decay of $C(t)$ apparently ceases, being replaced by an oscillation with stationary amplitude below
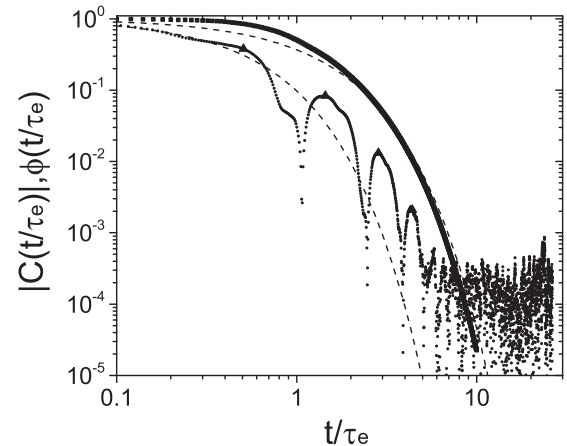

FIG. 5. Velocity autocorrelation function (dots) and survival probability (squares) for 0H billiards with $R_1 = 0.12L$ and $R_2 = 0.40L$; $\tau_e = 0.949$ and $a = 2.33 \pm 0.01$.
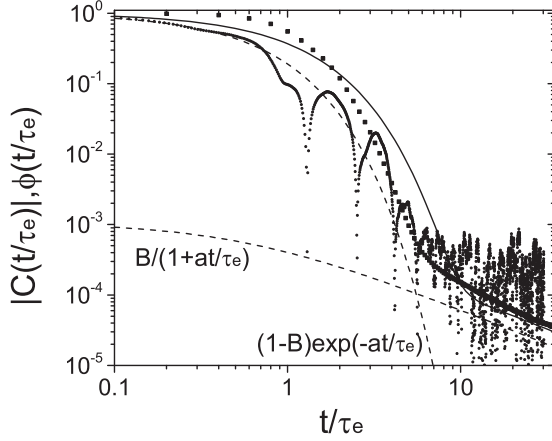
FIG. 6. Velocity autocorrelation function (dots) and survival probability (squares) for BB billiards with $R_1 = 0.08L$ and $R_2 = 0.40L$; $\tau_e = 0.825$.

FIG. 7. Diffusion coefficient of billiards between BB ($R_1 < R_c$) and 0H ($R_1 > R_c$). The values R_1 of the curves at reduced time are, from top to bottom, $0.50R_c$, $0.80R_c$, $1.00R_c$ (dashed line), $1.20R_c$, $1.60R_c$, and $2.00R_c$.

10^{-3}. This noiselike behavior has been assigned to numerical errors, whose main source is the finite number of initial conditions [36]. We assume that the decay has terminated together with the exponential fit. This exponential decaying behavior of $C(t)$ and $\phi(t)$ is expected for 0H billiards and is typical of hyperbolic systems [3,5,11,16,37].

The adjustment on the decay rate of $C(t)$ in Fig. 5 indicates τ_c as the characteristic relaxation time for $C(t)$, considering that $\tau_e/\tau_c = 2.18 \approx a$. This is expected since correlations are lost due to collisions with scatterers. Therefore, in the next figures, we use this correction to the characteristic time for $C(t)$ directly, instead of the best fit.

Below the transition, the bouncing balls corridors are open. Figure 6 shows the di-log plot of $C(t)$ (dots) and $\phi(t)$ (squares) for $R_1 = 0.80R_c$, which is a case with very narrow corridors. The dashed curves represent the main behavior of the decay of $C(t)$, evidencing an exponential decay as $(1 - B)e^{-at/\tau_e}$, and an asymptotic algebraic decay as $B/(1 + at/\tau_e)$, with $B = 1.07 \times 10^{-3}$, $\tau_e = 0.825$, $\tau_c = 0.497$, and $a = \tau_e/\tau_c$. As it was demonstrated in Fig. 5, the characteristic decay time for $C(t)$ is τ_c. $\phi(t)$ follows the behavior of the decay of $C(t)$, but its algebraic decay is more evident. The solid curve represents Eq. (14), using $\tau = \tau_e$. The difference between the curve and the points for $\phi(t)$, in short time, can be explained by the simulation strategy which accounts the flight time in the total surviving time. In short time, the flight time is in the same magnitude of the time for just having escaped from the original site. It suggests that the exponential part should be more complex than the one used in (14); however, it is a good model for a general behavior. The decay of $C(t)$ is mainly exponential and the $1/t$ contribution is very small and remains below the strong oscillations of $C(t)$ right after the end of the exponential decay. In fact, as shown by the value of B, the phase-space volume of the open corridors, in this case, is negligible in comparison to the whole phase space, meaning that though this billiard is classified geometrically as ∞H, some of its dynamical properties are similar to those of 0H billiards, which are hyperbolic systems. This is evidenced not only by the fast decay of $C(t)$ but also by the behavior of
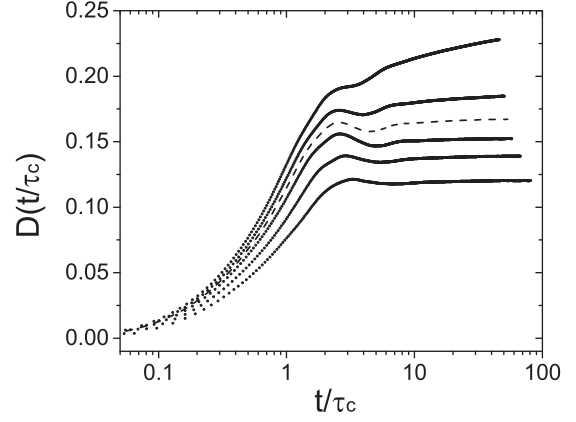
$D(t)$ which neither converges nor grows as quickly as other nonhyperbolic systems, as shown in Fig. 7.

We point out that as R_1 gets smaller, the nonhyperbolic properties get stronger, the $1/t$ tail is more visible above the long time oscillations of $C(t)$ and the diffusion coefficient grows faster. Such is the case of the $0.50R_c$ (a similar case is the $1.06R_c$, discussed in Sec. V C).

The time-dependent diffusion coefficients are shown in Fig. 7 with the values of R_1, from the top, $0.50R_c$, $0.80R_c$, $1.00R_c$ (dashed line), $1.20R_c$, $1.60R_c$, and $2.00R_c$. All the 0H cases seem to converge to a finite value. The $0.80R_c$ case grows very slowly indicating its weak nonhyperbolic properties, which get stronger in the $0.50R_c$ case. It is evident that the delay of the logarithmic growth of $D(t)$, in the $0.80R_c$ case, is due to the small value of B, as shown in (17). However, this delay implies that the macroscopic property $D(t)$ behaves like hyperbolic systems.

In this first set, we see that the dynamical properties of BB billiards, close to the transition from 0H, remain very similar to 0H, even though there are open corridors. This feature comes from the fact that the phase space of the bouncing balls corridors is drastically reduced by the presence of the second sublattice.

B. 0H to D

In the second set, the diagonal corridor is opened from 0H. We fix $R_1 = 0.20L$ and change R_2 to $1.06R_c$, $1.00R_c$, $0.92R_c$, $0.85R_c$, and $0.78R_c$ (represented by triangles in Fig. 3), where $R_c = \sqrt{2}/4L \approx 0.3536L$. Billiards above $1.00R_c$ are 0H, billiards between $0.85R_c$ and $1.00R_c$ are D and below $0.85R_c$ are billiards with both bouncing balls and diagonal corridors.

The $1.06R_c$ and $1.00R_c$ cases are 0H billiards with the same previously described properties in the Sec. V A. Figure 8 presents $C(t)$ and $\phi(t)$ for the $0.92R_c$ case, with the main diagonal open corridor. The decay starts exponentially and then continues algebraically, as evidenced by the dashed curves. The algebraic tail is characteristic of nonhyperbolic systems and is originated by the particles traveling along the open
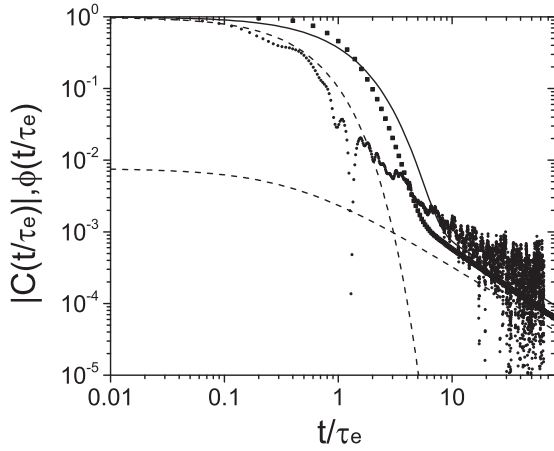
FIG. 8. Velocity autocorrelation function (dots) and survival probability (squares) for D billiards with $R_1 = 0.20L$ and $R_2 = 0.325L$. The dashed curves evidence the decay of $C(t)$ and the solid refers to the decay of $\phi(t)$, as in Fig. 6. $\tau_e = 1.17$.
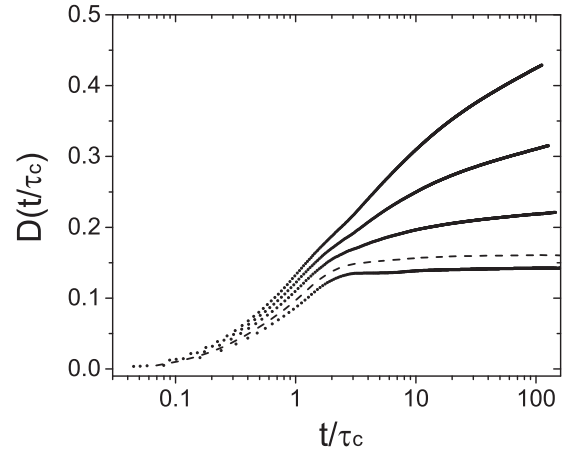

FIG. 10. Diffusion coefficient of billiards between ∞H ($R_2 < R_c$) and 0H ($R_2 > R_c$). The values of R_2 for the curves at long time are, from top to bottom, $0.78R_c$, $0.84R_c$, $0.92R_c$, $1.00R_c$ (dashed line), and $1.06R_c$.

corridors, suffering fewer collisions, and retaining correlations for longer times.

The algebraic tail is even more evident in the $0.78R_c$ case, as shown in Fig. 9. In this case, both the diagonal and bouncing balls corridors are open and the contribution of each one is evidenced by the dashed curves, being the D curve the diagonal algebraic decay with $B = 0.049$ and the BB curve the bouncing balls with $B = 0.001$, which is a negligible contribution.

The diffusion coefficient calculated for this set is shown in Fig. 10. The three nonconverging curves at the top are the nonhyperbolic systems (∞H), while the two curves at the bottom are the hyperbolic systems (0H, including the transition case), which converge to a finite value. Different from BB, the diagonal corridors exhibit nonhyperbolic characteristics right after finishing 0H.

C. ∞H to BB

In the third set, we focus on the transition by closing the diagonal corridors and keeping only the bouncing balls corridors open. We fix $R_1 = 0.05L$ and change R_2 to $0.78R_c$, $0.92R_c$, $1.00R_c$, and $1.06R_c$, where $R_c = \sqrt{2}/4L \approx 0.3536L$ (represented by the circles in Fig. 3). In this case, billiards below R_c have multiple types of corridors, while above R_c they have only BB corridors, as in the first set in Sec. V A.

The $0.92R_c$ case shown in Fig. 11 is clearly nonhyperbolic and is very similar to its equivalent in set 2. In this case, the BB dashed curve is related to the bouncing balls corridor, with the relative volume $B = 0.031$ and the D curve is related to the diagonal corridor with $B = 0.006$. Figure 12 displays $C(t)$ and $\phi(t)$ for the $1.06R_c$ case where only the bouncing balls corridors are open. We see that in the limit close to the opening of the diagonal corridor the bouncing balls corridors are large enough to display the algebraic tail,
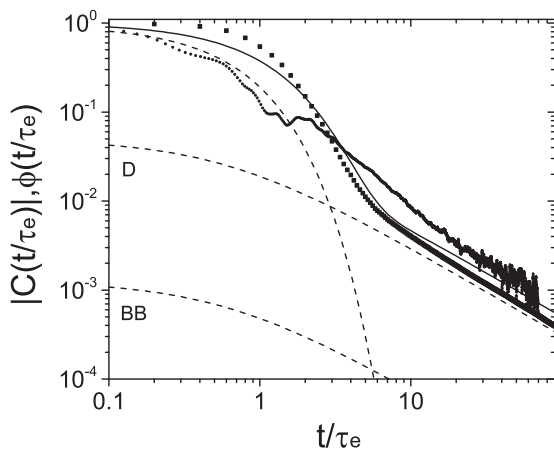

FIG. 9. Velocity autocorrelation function (dots) and survival probability (squares) for ∞H billiards with $R_1 = 0.20L$ and $R_2 = 0.275L$. The top (D) dashed curve refers to the diagonal corridors algebraic decay and the bottom (BB) to the bouncing balls corridors. $\tau_e = 1.08$.
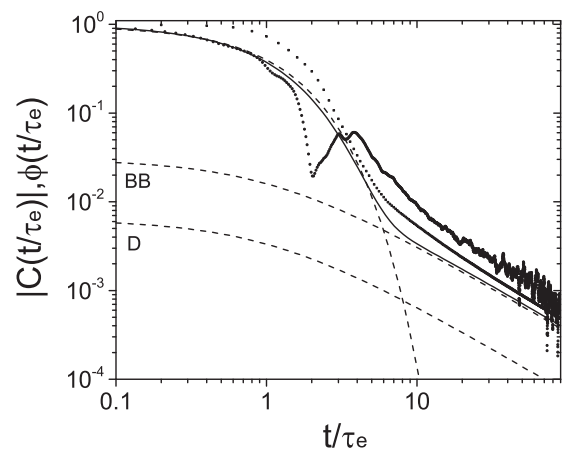

FIG. 11. Velocity autocorrelation function (dots) and survival probability (squares) for ∞H billiards with $R_1 = 0.05L$ and $R_2 = 0.325L$. The top (BB) dashed curve refers to the bouncing balls corridors algebraic decay and the bottom (D) to the diagonal corridors. $\tau_e = 0.78$.
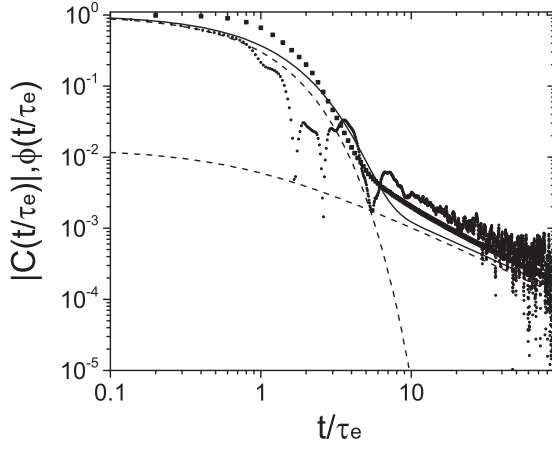
FIG. 12. Velocity autocorrelation function (dots) and survival probability (squares) for BB billiards with $R_1 = 0.05L$ and $R_2 = 0.375L$. $\tau_e = 0.77$.

with relative volume of $B = 0.013$. The diffusion coefficient for this configuration is shown in Fig. 13, where every case in this set diverges logarithmically, though the growing rate decreases significantly when the diagonal corridor is closed.

The smooth transition between 0H and ∞H billiards was already shown by Friedman and Martin [13] and then by Matsuoka and Martin in a triangular lattice billiards [12]. Since our double square lattice provides the freedom to isolate either type of open corridors, we can separately analyze their effects. As mentioned before, our results in Fig. 9 show little contribution of the bouncing balls corridors to the algebraic tail of $C(t)$. This is explained by the small relative phase-space volume of the open corridors, leading to a very slow transition from hyperbolic to nonhyperbolic. The diagonal open corridors have a larger phase-space volume and the algebraic tail is visible right after the transition from 0H. If both types of corridors are open, then the algebraic tail is clearly visible and the disk radii can be adjusted to choose which type of corridor has a greater volume, as depicted in Figs. 9 and 11.
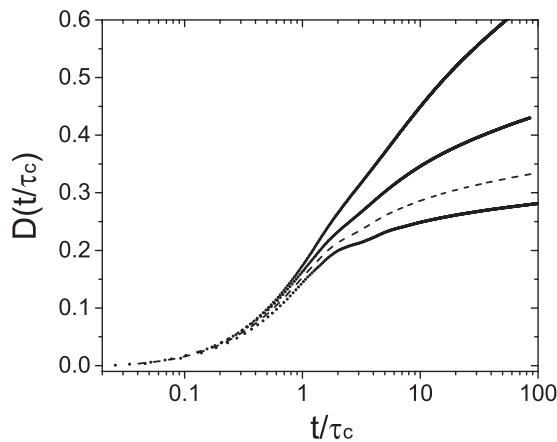

FIG. 13. Diffusion coefficient of billiards between ∞H ($R_2 < R_c$) and BB ($R_2 > R_c$). The values of R_2 for the curves at long time are, from top to bottom, $0.78R_c$, $0.92R_c$, $1.00R_c$ (dashed line), and $1.06R_c$.
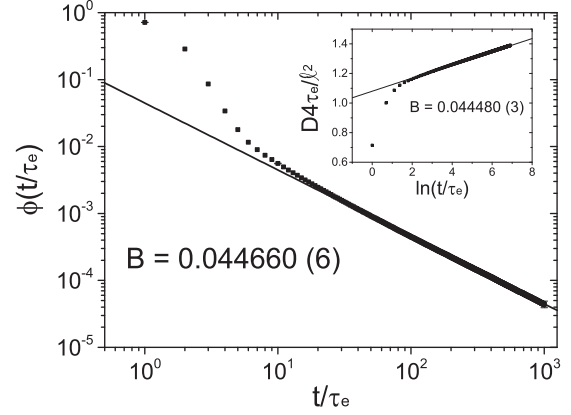

FIG. 14. Fitting of the algebraic part of $\phi(t)$, according to (14). The data points refer to the configuration $R_1/L = 0.05$ and $R_2/L = 0.325$. The small error bars are included for some points. The inset shows the equivalent points for diffusion coefficient, obtained by (13). In both data, the fitting was performed to the points in the time range between 10^2 and 10^3 t/τ_e.

D. Dynamical transitions

In our simulations we have used $C(t)$ instead $\phi(t)$ to calculate $D(t)$ to avoid the characteristic parameters τ and ℓ; however, $\phi(t)$ is better suited to evaluate the long-time behavior of $D(t)$. We concentrate in analyzing the B coefficient as the parameter that characterizes this long-time behavior in nonhyperbolic billiards [Eq. (17)], without the necessity of determining τ and ℓ. It is possible to calculate B directly from the algebraic part of $\phi(t)$ [Eq. (14)]. Figure 14 shows the data points for one of the configurations in the third set, presented in Sec. V C, with $R_1/L = 0.050$ and $R_2/L = 0.325$. The coefficient $B = 0.044660 \pm 6 \times 10^{-6}$ was calculated using the best fit for the function $B/(t/\tau_e)$ in the range between 10^2 and 10^3 t/τ_e, represented by the continuous line. With these same data points, in the inset, $D(t)$ was calculated using (13), with $B = 0.044480 \pm 3 \times 10^{-6}$ fitted by the function $A + B \ln(t/\tau_e)$ in the same time range. Considering that there is no significant difference between the two B values, in the following Figs. 15 and 16, we use B calculated from $\phi(t)$.

The data points of B in relation to the geometrical parameter R_2/L are shown in Fig. 15 for the billiards of the third set, presented in Sec. V C, with fixed $R_1/L = 0.05$ and varying R_2/L from one region with two open corridors (D and BB) to another region with only one open corridor (BB). The segmented line separates the regions in the point $R_2/L = \sqrt{2}/4$. The dotted lines represent the theoretical values, according to (15), for BB and D corridors separately, and the continuous line represents their sum (total B). Despite the points and continuous line do not perfectly match (error bars are smaller than the points), (15) is a worthy theoretical prediction. Observe that the total B, represented by the continuous line, is sensitive to the transition between the two regions separated by the segmented line. The inset shows the derivative of B in relation to R_2, where it is possible to observe the change of slope in the transition point. Besides the fact that B distinguishes hyperbolic ($B = 0$) and nonhyperbolic ($B > 0$) billiards, its sensitivity is more refined, showing the closure of corridors. The dynamical transition, when all corridors close, was described as thermodynamic
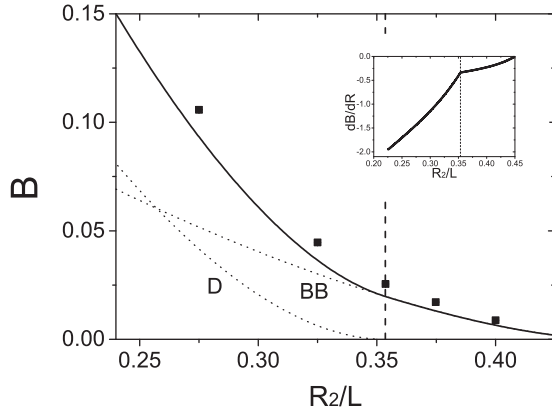
FIG. 15. Weight B of algebraic part of $\phi(t)$ in function of the radius R_2. The data points refer to the third set of configurations analyzed in Sec. V C. The dotted lines represent the theoretical values of B, according to (15), for BB and D corridors with fixed R_1. The continuous line is the sum of them. The segmented line marks the value of R_2 from which the D corridors close. The error bars are smaller than the points. The inset shows the derivative of the continuous line.

phase transition by Gaspard and Baras [14] by analyzing the behavior of the derivative of the pressure function. Different phases differ in all thermodynamic properties, including the isothermal compressibility, κ_T ($T/V\kappa_T = -\partial^2 S/\partial V^2$), where T is the temperature. The necessity of the entropy S to be a homogeneous first-order function of the extensive parameters allows us to include B parameter as $S(V) = S(BV)/B$ [38]. Derivatives of entropy implies in derivatives of B. And derivatives with respect to volume V is also a derivative with respect to R, because the thermodynamic volume V in our model is equivalent to the area $L^2 - \pi(R_1^2 + R_2^2)$ of the billiard table. The plot in the inset of Fig. 15 suggests that other phase transitions seem to exist.
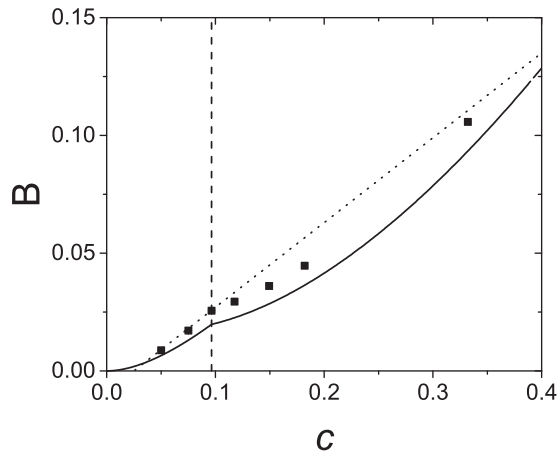

FIG. 16. Weight B of algebraic part of $\phi(t)$ in function of width c of BB corridors. The data points are the same configurations as in Fig. 15. The continuous line represents the theoretical values of B, according to (15), summing the contribution of BB and D corridors with fixed R_1. The segmented line marks the value of c from which D corridors open. The dotted line represents the linear dependence proposed in Ref. [25]. The error bars are smaller than the points.

When there are no open corridors, the particles only collide with neighboring scatterers and their movement across the lattice is a composition of small jumps between neighboring sites. These continuous collisions result in all the trajectories in phase space to be classified in just one state, called scattering phase in Ref. [25], characterized by the escape time τ_e [Eq. (4)]. When there are open corridors, apart from the scattering phase, the particles moving inside these corridors establish a special group of trajectories in phase space, called propagation phase in Ref. [25], which suggests a characteristic time τ_F proportional to the mean free path ℓ. Following this suggestion, the mean time between jumps could be expressed by

$$\tau = \tau_e + A\ell, \tag{22}$$

where the first term is the mean time that the particles spend in a site and the second, the mean time to move to another site, with A being a constant. For 0H billiards, $\tau_e \gg A\ell$ and $\tau \approx \tau_e$. However, for ∞H billiards, the group of particles in corridors, flying across the lattice until arriving at another site, could not have a characteristic time. It is possible that the mean length of jumps and the mean time between jumps, as defined in (9) and (10), can diverge in long time for ∞H billiards. This problem can be transferred to diffusion coefficient as $D = \langle r^2 \rangle / 4\langle t \rangle$, where the ratio of the mean values

$$\frac{\langle r^2 \rangle}{\langle t \rangle} = \frac{\ell^2}{\tau_e}\left\{1 + B\left[\ln\left(\frac{t}{\tau_e}\right) - 2\right]\right\} \text{ (for } t \gg \tau_e)$$

carry the divergence to the diffusion coefficient, when $B > 0$ [see (17)].

We would like to point out the major difference between our results and the Ref. [25]. In our proposal (15), we consider B to be proportional to the relative phase-space volume of each open corridor. In Fig. 16, we organize a parametric plot of B in relation to the width c of the corridors, being both B and c functions of the radii R_1 and R_2. The simulation points are calculated in the set of Sec. V C, with fixed R_1 and varying R_2 to observe the transition from one open corridor (BB) to two open corridors (D and BB), including two additional points, with $c = 0.119$ ($R_2 = 0.98R_c$) and $c = 0.149$ ($R_2 = 0.95R_c$). The continuous line is the theoretical values [Eq. (15)], with the contribution of two open corridors. The segmented line indicates the point where D corridors open. Similarly as in Fig. 15, the theoretical prevision does not perfectly match the data points, but properly follows their behavior. The dotted line represents the linear dependence similar to the proposal in Ref. [25]. We use the best linear fit using the first three points, with $B = 0.36c - 0.0094$. The authors in Ref. [25] use a simpler geometry than we do and observe the system in the limit of narrow corridors. They suggest $B = c/\ell$, with $\ell = 1$. In a direct comparison, ℓ would be equivalent to 2.8 in our system. However, Fig. 16 indicates that a parabolic relation with c is more appropriate. In addition, we propose in the end of the Sec. III to express $B = c/\tau_t$, where τ_t is the transition time from scattering to propagating states [Eq. (18)]. This mean time exists only in ∞H systems and characterizes different corridors.

Considering that many characteristic times appear on this paper, we list them in Table I. This variety of characteristic times suggests that many processes occur in the periodic Lorentz gas. The Lorentz gas is primarily a deterministic

TABLE I. Characteristic times.

Symbol	Description	Related Quantity
τ_c	Collision time [Eq. (21)]	Velocity autocorrelation function
τ_t	Transition time [Eq. (18)]	Diffusion coefficient (logarithmic part)
τ	Time between jumps [Eq. (22)]	Diffusion coefficient (linear part)
τ_e	Escape time [Eq. (4)]	Survival probability

system; however, the dispersive nature of its trajectories allows us to deal with the length of jumps and the time between jumps as random variables and to introduce stochastic approaches [22]. τ is the only characteristic time introduced in this paper related to the stochastic approach [Eq. (10)]. The remaining times are defined in a deterministic context, all derived from (3). The microscopic processes are characterized by the collision time τ_c and all the billiard dynamic properties are revealed after this time. τ_t appears only in ∞H billiards, whose nonhyperbolic properties are exposed after this characteristic time. τ and τ_e were defined in the context of the diffusion process. τ is the natural mean time to characterize the movement across the lattice and characterizes the macroscopic process. But since $\tau \approx \tau_e$ in 0H billiards and it is not defined in ∞H billiards, τ_e has been used as a reference time. Therefore, for 0H billiards and for ∞H billiards, in the limit of narrow corridors, $\tau_e > \tau_c$ and they distinguish macroscopic and microscopic processes, respectively. And the complete characterization of the diffusion process occurs for $t \gg \tau_e$. The movement of the particles on the lattice is independent of the presence of open corridors. The particles can move through the lattice and remain in their collisional state. For this reason, $\tau_t > \tau_e$ when one kind of corridors is open, meaning that the particles can spend more time to escape from the collisional state than to escape from a site, in ∞H billiards.

VI. CONCLUSIONS

In this paper we have numerically studied the velocity autocorrelation function $C(t)$, the survival probability $\phi(t)$, and the diffusion coefficient $D(t)$ on a double square lattice Lorentz gas. Our particular interest was in the dynamical transitions and properties of each horizon type, ∞H and 0H, allowed by the adjustment of the sublattices radii.

By isolating each type of corridor, we were able to distinguish its influence on the dynamical properties of the billiards. In BB billiards, where there are only vertical and horizontal corridors, near the transition to 0H, we find that $D(t)$, calculated from $C(t)$, reflects very similar dynamics to 0H billiards. This is a consequence of the statistical oscillations of $C(t)$ when they begin before the algebraic tail and mask the anomalous behavior of $D(t)$. Both the logarithmic growth of $D(t)$ and the algebraic tail of $C(t)$ are weighed by the geometric parameter B, which is very small near the transition. However, $\phi(t)$ is sensitive enough to show the algebraic tail even near

the transition, since it has no oscillations, and it is possible to calculate the values of B from it. In the D case, the open corridors volume B in the phase space is larger than in the BB case, showing the algebraic tail right after the transition from 0H. If both corridors are open simultaneously, then the influence of each corridor to the algebraic tail can be modulated by adjusting the disks radii (Figs. 9 and 11).

In our stochastic model, $\phi(t)$ takes the equivalent role of $C(t)$ in the diffusion coefficient derivation [Eq. (13)] and both quantities have similar behavior in relation to their decays, as shown by our results. This suggests that $\phi(t)$ and $C(t)$ have the same origin within the dynamics of the billiards and there might be a direct relation between them, which connects the stochastic and deterministic models. Using a linear combination of exponential and algebraic functions to represent $\phi(t)$, it was possible to derive the diffusion coefficient in (17) displaying both normal and anomalous diffusions according to the geometric parameter B. The normal term of this equation accounts for the time that the particles spend trapped on a site colliding with the scatterers, whereas the anomalous term accounts for particles that leave the traps via open corridors and may have long ballistic trajectories before colliding with another scatterer. These particles originate the algebraic tail in both $\phi(t)$ and $C(t)$. However, $\phi(t)$ decays on a time scale given by τ_e which is related to the escape rate of the particles from a site, whereas $C(t)$ decay is ruled by the mean collision time, τ_c.

The parameter B is sensitive to a dynamical transition from nonhyperbolic to hyperbolic billiards, which has been treated as a phase transition, like in a thermodynamics approach [14]. Analyzing the derivative of B in relation to R, the change of the slope at the geometric transition, when there are two kinds of open corridors to one kind of open corridors (BB and D together to BB alone), might suggest the presence of other phase transitions in the nonhyperbolic regime. The open corridors in ∞H billiards allow the coexistence of distinct states in phase space for long time. This composite structure of the phase space fosters the complex behavior of the Lorenz gas, which deserves further studies.
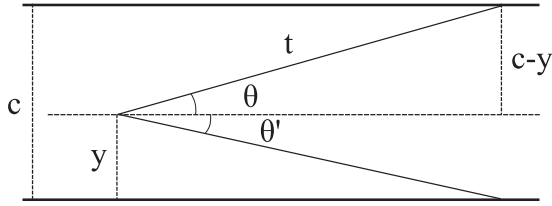
APPENDIX A

In the sense of making the limit in (8) to obtain (11), after derivation, it is necessary to define

$$\Omega(u) \equiv \int \Psi(r,u)\, d\mathbf{r}, \tag{A1}$$

$$\Xi^2(u) \equiv \int r^2 \Psi(r,u)\, d\mathbf{r}, \tag{A2}$$

and to consider that

$$\int \mathbf{r}\, \Psi(r,u)\, d\mathbf{r} = 0 \tag{A3}$$

FIG. 17. Schematic representation of an open corridor of width c.

and the limits

$$\lim_{k \to 0} \Psi(\mathbf{k}, u) = \Omega(u), \tag{A4}$$

$$\lim_{k \to 0} \frac{\partial \Psi(\mathbf{k}, u)}{\partial k} = 0, \tag{A5}$$

$$\lim_{k \to 0} \frac{\partial^2 \Psi(\mathbf{k}, u)}{\partial k^2} = \Xi^2(u). \tag{A6}$$

The next step for (8) is

$$\lim_{k \to 0} \frac{\partial^2 W(\mathbf{k}, u)}{\partial k^2} = \Phi(u) \left\{ \frac{-\Xi^2(u)}{[1 - \Omega(u)]^2} \right\}. \tag{A7}$$

Now we consider asymptotic forms for $\Omega(u)$ and $\Xi^2(u)$ for small u, which corresponds to large t,

$$\Omega(u) \approx \int_0^\infty dt (1 - ut) \int d\mathbf{r} \, \psi(r, t)$$
$$= 1 - u\tau, \tag{A8}$$

$$\Xi^2(u) \approx \int d\mathbf{r} \, r^2 \int_0^\infty dt \, \psi(r, t) = \ell^2 \tag{A9}$$

where we use (9) and (10).

The final result, considering $t \gg \tau$, is

$$\lim_{k \to 0} \frac{\partial^2 W(\mathbf{k}, u)}{\partial k^2} = \frac{-\ell^2}{\tau^2} \frac{\Phi(u)}{u^2}. \tag{A10}$$

APPENDIX B

Consider a billiard with an open corridor of a single type (either bouncing balls or diagonal) of width c and a particle that travels in this corridor up to a time t before a collision, represented in Fig. 17. The phase-space volume of this corridor is the result of the integration

$$\int_0^{t \cos \theta} dx \int_0^c dy \int_{\theta'}^{\theta} d\theta. \tag{B1}$$

If t is large, then we consider $\theta \approx \sin \theta = (c - y)/t$, $\cos \theta \approx 1$, and $\theta' \approx \sin \theta' = -y/t$, so the integration is

$$\int_0^t dx \int_0^c dy \int_{\frac{-y}{t}}^{\frac{c-y}{t}} d\theta = c^2. \tag{B2}$$

Since a billiard cell contains four corridors with two directions each, the result is multiplied by 8. The ratio between this volume and the whole phase space of the billiard gives the value of B in (15).

[1] P. Gaspard and G. Nicolis, Phys. Rev. Lett. **65**, 1693 (1990).

[2] H. A. Lorentz, The motion of electrons in metallic bodies I, *Proceedings of KNAW*, Vol. 7 (North-Holland, Amsterdam, 1905), pp. 438–453.

[3] L. Bunimovich and Y. Sinai, Commun. Math. Phys. **78**, 479 (1981).

[4] J. Machta and R. Zwanzig, Phys. Rev. Lett. **50**, 1959 (1983).

[5] B. Friedman and R. Martin Jr., Phys. Lett. A **105**, 23 (1984).

[6] P. Bleher, J. Stat. Phys. **66**, 315 (1992).

[7] N. Chernov and S. Troubetzkoy, J. Stat. Phys. **83**, 193 (1996).

[8] N. Chernov, J. Stat. Phys. **88**, 1 (1997).

[9] P. Cvitanović, P. Gaspard, and T. Schreiber, Chaos **2**, 85 (1992).

[10] P. L. Garrido and G. Gallavotti, J. Stat. Phys. **76**, 549 (1994).

[11] A. J. Fendrik and M. J. Sánchez, Phys. Rev. E **51**, 2996 (1995).

[12] H. Matsuoka and R. Martin Jr., J. Stat. Phys. **88**, 81 (1997).

[13] B. Friedman and R. Martin Jr., Physica D **30**, 219 (1988).

[14] P. Gaspard and F. Baras, Phys. Rev. E **51**, 5332 (1995).

[15] W. Bauer and G. F. Bertsch, Phys. Rev. Lett. **65**, 2213 (1990).

[16] A. J. Fendrik, A. M. F. Rivas, and M. J. Sánchez, Phys. Rev. E **50**, 1948 (1994).

[17] H. Alt, H.-D. Gräf, H. L. Harney, R. Hofferbert, H. Rehfeld, A. Richter, and P. Schardt, Phys. Rev. E **53**, 2217 (1996).

[18] V. Kokshenev and M. Nemes, Physica A **275**, 70 (2000).

[19] E. Vicentini and V. Kokshenev, Physica A **295**, 391 (2001).

[20] V. B. Kokshenev and E. Vicentini, Phys. Rev. E **68**, 016221 (2003).

[21] R. Klages and C. Dellago, J. Stat. Phys. **101**, 145 (2000).

[22] T. Gilbert and D. P. Sanders, Phys. Rev. E **80**, 041121 (2009).

[23] C. Angstmann and G. Morriss, Phys. Lett. A **376**, 1819 (2012).

[24] G. Cristadoro, T. Gilbert, M. Lenci, and D. P. Sanders, Phys. Rev. E **90**, 022106 (2014).

[25] G. Cristadoro, T. Gilbert, M. Lenci, and D. P. Sanders, Phys. Rev. E **90**, 050102 (2014).

[26] M. Gutzwiller, *Chaos in Classical and Quantum Mechanics*, Interdisciplinary Applied Mathematics (Springer, New York, 1991).

[27] C. F. Hillermeier, R. Blümel, and U. Smilansky, Phys. Rev. A **45**, 3486 (1992).

[28] G. Casati, I. Guarneri, and G. Maspero, Phys. Rev. Lett. **84**, 63 (2000).

[29] L. Kadanoff, *Statistical Physics: Statics, Dynamics and Renormalization* (World Scientific, Singapore, 2000).

[30] R. Metzler and J. Klafter, Phys. Rep. **339**, 1 (2000).

[31] J. Klafter, A. Blumen, G. Zumofen, and M. Shlesinger, Physica A **168**, 637 (1990).

[32] E. Butkov, *Mathematical Physics* (Addison-Wesley, London, 1968).

[33] D. I. Dolgopyat and N. I. Chernov, Russ. Math. Surv. **64**, 651 (2009).

[34] ξ_{flow} is the variance of the random variable $\mathbf{r}(t)/\sqrt{t \log t}$.

[35] The first point (0.01054, 0.9998) was used in the fit but does not appear in the figure .

[36] This result is coherent with the statistical error of $C(t)$ which is proportional to inverse square root of initial condition [12,13,37]. In our case this error is $1/\sqrt{2 \times 10^7} \approx 2 \times 10^{-4}$.

[37] J. Machta and B. Reinhold, J. Stat. Phys. **42**, 949 (1986).

[38] H. Callen, *Thermodynamics and an Introduction to Thermostatistics*, 2nd ed. (Wiley, New York, 1985).